HHS Public Access

Author manuscript

Nat Neurosci. Author manuscript; available in PMC 2015 July 07.

Published in final edited form as:

Nat Neurosci. ; 14(8): 1017–1022. doi:10.1038/nn.2844.

Zinc alleviates pain through high-affinity binding to the NMDA receptor NR2A subunit

Chihiro Nozaki[1,2,3,4,8], **Angela Maria Vergnano**[5,6,7,8], **Dominique Filliol**[1,2,3,4], **Abdel-Mouttalib Ouagazzal**[1,2,3,4], **Anne Le Goff**[5,6,7], **Stéphanie Carvalho**[5,6,7], **David Reiss**[1,2,3,4], **Claire Gaveriaux-Ruff**[1,2,3,4], **Jacques Neyton**[5,6,7], **Pierre Paoletti**[5,6,7,9], and **Brigitte L Kieffer**[1,2,3,4,9]

[1]Institut de Génétique et Biologie Moléculaire et Cellulaire, Illkirch, France

[2]Centre National de la Recherche Scientifique (CNRS) UMR7104, Illkirch, France

[3]Institut National de la Santé et de la Recherche Médicale (INSERM) U964, Illkirch, France

[4]Université de Strasbourg, Illkirch, France

[5]Ecole Normale Supérieure, Institut de Biologie de l'Ecole Normale Supérieure, Paris, France

[6]CNRS UMR8197, Paris, France

[7]INSERM U1024, Paris, France

Abstract

Zinc is abundant in the central nervous system and regulates pain, but the underlying mechanisms are unknown. *In vitro* studies have shown that extracellular zinc modulates a plethora of signaling membrane proteins, including NMDA receptors containing the NR2A subunit, which display exquisite zinc sensitivity. We created NR2A-H128S knock-in mice to investigate whether Zn^{2+}–NR2A interaction influences pain control. In these mice, high-affinity (nanomolar) zinc inhibition of NMDA currents was lost in the hippocampus and spinal cord. Knock-in mice showed hypersensitivity to radiant heat and capsaicin, and developed enhanced allodynia in inflammatory and neuropathic pain models. Furthermore, zinc-induced analgesia was completely abolished under both acute and chronic pain conditions. Our data establish that zinc is an endogenous modulator of excitatory neurotransmission *in vivo* and identify a new mechanism in pain processing that relies on NR2A NMDA receptors. The study also potentially provides a molecular basis for the pain-relieving effects of dietary zinc supplementation.

Correspondence should be addressed to P. P. (pierre.paoletti@ens.fr).

[8]These authors contributed equally to this work.

[9]These authors jointly directed this work.

AUTHOR CONTRIBUTIONS

B.L.K. and P. P. designed and supervised the study. D.F., J.N. and A.L.G. contributed to the creation NR2A-H128S mutant mouse line. J.N. and P.P. performed the electrophysiologial experiments on *Xenopus* oocytes. A.M.V. ran electrophysiological characterization of mutant mice and performed the Timm's staining. C.N. performed all of the pain experiments. D.R. and A.-M.O. conducted neurological examination of mutant mice. S.C. and A.M.V. performed immunochemistry. C.G.-R. and J.N. contributed to conceptual aspects of the study. C.N., A.M.V., C.G.-R., A.-M.O., P.P. and B.L.K. wrote the manuscript.

COMPETING FINANCIAL INTERESTS

The authors declare no competing financial interests.

Note: Supplementary information is available on the Nature Neuroscience website.

Zinc is essential for life and is the second most prevalent trace element in the body, after iron. This heavy metal is crucially involved in cellular metabolism, and detrimental consequences of zinc deficiency in human nutrition and public health have been well recognized since the 1960s[1]. Most zinc is bound to metalloproteins and contributes to enzymatic catalysis or structural stability[1]. Zinc is particularly abundant in the CNS. A substantial amount of neural zinc (~10%) is found in axon terminals of neurons in a chelatable ionic form (Zn^{2+})[2]. CNS chelatable Zn^{2+} is mostly sequestered in synaptic vesicles of glutamatergic neurons, and release of Zn^{2+} with glutamate has been proposed to modulate both excitatory and inhibitory synaptic transmission and plasticity[3–6]. This observation led many authors to propose a role for zinc in brain functions, such as motor control[7], and in neurological disorders[2,8], including in pathological pain[9,10]. At present, however, the physiological importance of synaptic zinc remains largely unknown. A major hurdle in the study of synaptic zinc physiology is the myriad of potential zinc targets, which include several voltage-dependent ion channels and principal neurotransmitter transporters and receptors[8,11–13]. On these targets, zinc can exert either positive or negative modulatory effects with degrees of potency that vary considerably. Effects of zinc are thus expected to be many and complex, both increasing and decreasing neuronal excitability.

In vitro, NMDA receptors (NMDARs) have been identified as one of the potential synaptic targets for zinc effects on excitatory transmission[11,13]. NMDARs have key roles in both the physiology and pathology of the nervous system[14]. Notably, these receptors contribute to pain transmission and the development of chronic pain[15,16]. NMDARs are heteromeric assemblies composed mainly of NR1 and NR2 subunits, and they form glutamate-gated ion channels with biophysical and pharmacological properties largely determined by the type of NR2 subunit: type A, B, C or D[14]. In particular, the NR2A subunit, which is widely expressed in the adult nervous system, confers to NMDARs an exquisite sensitivity for extracellular zinc. The NR2A clamshell-like N-terminal domain contains a high-affinity Zn^{2+} binding site, which mediates allosteric inhibition of NR2A-containing NMDARs by nanomolar zinc concentrations[17,18]. Functional and modeling studies on recombinant NMDARs have identified several residues that are essential for Zn^{2+} binding to the NR2A N-terminal domain. This is the case for His128, whose mutation strongly reduces Zn^{2+} affinity (a ~1,000-fold shift in the half-maximum inhibitory concentration), whereas other receptor properties—including agonist (glutamate and glycine) sensitivity, channel maximal open probability, Mg^{2+} block and proton inhibition—are unaffected[18–21]. To investigate the importance of zinc action on NMDARs *in vivo*, we generated mutant mice carrying the H128S mutation on the NMDAR NR2A subunit. Here, we show that the Zn^{2+}–NR2A interaction is a key molecular event that regulates major aspects of pain processing.

RESULTS

Generation and characterization of NR2A H128S knock-in mice

We generated knock-in mutant mice harboring a histidine-to-serine point mutation at position 128 of the NR2A subunit (NR2A-H128S mutation) to assess the physiological relevance of Zn^{2+} acting at NR2A subunits *in vivo*. We used homologous recombination to

introduce the desired mutation into the NR2A gene of mouse embryonic stem cells[22] and obtained the NR2A-H128S knock-in mouse line (Fig. 1).

We first assessed the effects of the NR2A-H128S mutation at the tissue level (Fig. 2). To determine whether NMDARs from NR2A-H128S mutant mice are insensitive to low (nanomolar) zinc concentrations, we transplanted forebrain membrane extracts into *Xenopus laevis* oocytes and measured resulting NMDA currents. High-affinity zinc inhibition of NMDA currents was lost (Fig. 2a), demonstrating that the targeting strategy was successful. Furthermore, sensitivity to ifenprodil, an NR2B-selective antagonist[14], was indistinguishable between wild-type (WT) and knock-in preparations, indicating that proportions of NR2A versus NR2B subunits were maintained in mutant mice (Fig. 2a). We then measured NMDA excitatory postsynaptic currents (EPSCs) in acute slices from the hippocampus, which possesses zinc-containing neuron terminals at high density[2,8], and from the spinal cord, which is a main site for pain processing. In both slice preparations, and in line with our observation in oocytes, NMDA EPSCs from WT mice were markedly inhibited by exogenous submicromolar zinc applications, whereas NMDA EPSCs from knock-in mice were barely affected (Fig. 2b). Hence, the NR2A-H128S mutation ablates high-affinity zinc modulation of NMDARs *in vivo*. Together, these data provide unambiguous evidence that NMDARs endogenously expressed in their native synaptic environment are highly sensitive to extracellular zinc, as previously shown in recombinant systems[17].

In contrast to these robust effects on zinc sensitivity, the mutation did not alter expression levels, in either the forebrain or spinal cord, of NR2A, NR2B or NR1 subunits, or those of AMPA receptors (GluR1 subunit), glycine receptors (GlyRα1 subunit) or the vesicular zinc transporter (ZnT3 (ref. 23)) (Fig. 2c and Supplementary Figs. 1 and 2). Moreover, the NR2B-selective antagonist Ro256981 (ref. 14; 1 μM) inhibited knock-in and WT hippocampal NMDA EPSCs to the same extent (percentage of inhibition: 47 ± 2% (n = 4) for knock-in versus 53 ± 3% (n = 3) for WT, P = 0.19, Student's t-test) revealing that the proportion of synaptic NR2A- versus NR2B-containing NMDA receptors was unaltered in mutant mice. Similarly, the presence of the NR2A-H128S mutation did not significantly change the synaptic time course of hippocampal NMDA EPSCs (P = 0.9, Student's t-test; Supplementary Fig. 3a). Furthermore, Timm's staining, which labels chelatable zinc, was identical in brain sections from knock-in and WT mice (Supplementary Fig. 3b). Thus, high-affinity zinc modulation of NMDARs was specifically eliminated in NR2A-H128S mice, whereas the abundance of main excitatory glutamate receptors, the inhibitory glycine receptor (another target of zinc[7]) and synaptic zinc remained unaltered.

Pain responses in NR2A-H128S knock-in mice

We conducted neurological examinations of NR2A-H128S mice. Mutants showed a general health comparable with WT mice (well groomed coats and normal body posture, muscle strength, body weight, body temperature, general sensory functions—including olfactory, auditory and visual functions—food consumption and locomotor exploration (Supplementary Table 1)). In addition, locomotor habituation in a novel environment and the circadian pattern of locomotor behavior were indistinguishable between mutants and

controls (Supplementary Fig. 4). Altogether, no major signs of behavioral abnormalities were detected in NR2A-H128S mutant mice.

To investigate whether endogenous Zn^{2+} binding to NR2A subunits is involved in pain control, we examined pain sensitivity in mutant mice (Fig. 3). Acute nociception in tail immersion and hot plate tests (Fig. 3a,b), as well as tail pressure and von Frey tests (Fig. 3e,f) were unchanged, but mutant mice showed increased responses to radiant heat (tail flick and Hargreaves tests) (Fig. 3c,d). This hypersensitivity was observed only at heat rates of 0.9 or 2.2 °C s^{-1} but not at 4.0 °C s^{-1} (Fig. 3g), revealing a thermal hypersensitivity under slow heat pain stimulation. The mechanisms underlying responses to distinct pain stimuli are complex and recruit multiple primary afferent neurons[24]. Slow heating conditions (tail flick test at 0.9 or 2.2 °C s^{-1} and Hargreaves test) mainly stimulate nociceptive C fibers, whereas fast heating conditions (tail flick test at 4.0 °C s^{-1}, tail immersion and hot plate tests) preferentially recruit Aδ fibers[25,26]. Altogether, these observations suggest that endogenous Zn^{2+} binding to NR2A subunits inhibits C fibers rather than Aδ fibers. This is consistent with the notion that excitation of C fibers, but not Aδ fibers, leads to increased NMDAR function in target spinal cord neurons[16,27].

To further investigate the involvement of C and Aδ fibers, we tested mutant mice for tonic pain responses induced either by capsaicin (a TRPV1 activator that preferentially activates unmyelinated C fibers) and TIP39 (a parathyroid hormone 2 receptor agonist that selectively activates myelinated nociceptive A fibers)[28]. NR2A-H128S mice showed clear hypersensitivity to capsaicin but not to TIP39 (Fig. 3h–j), indicating that disruption of the Zn^{2+}-NR2A interaction enhances C-fiber excitability. Therefore, endogenous Zn^{2+} binding to NR2A limits NMDAR-regulated excitability mainly at the level of C fibers.

As NMDA receptors are important actors of chronic pain development[15,16], we examined chronic pain responses of NR2A-H128S mice. We used two well established models of chronic pain, namely complete Freund's adjuvant (CFA)-induced inflammatory pain and partial sciatic nerve ligation (SNL)-induced neuropathic pain (Fig. 4). In WT mice, both CFA intraplantar administration and SNL induced significant ($P < 0.001$, Student's *t*-test) hypersensitivity to heat (heat hyperalgesia in the Hargreaves test) and tactile stimuli (mechanical allodynia in von Frey measures). In mutant mice, thermal sensitivity to radiant heat was higher at the basal state under both conditions, as observed in the acute pain experiments. However, after CFA and SNL, heat hyperalgesia developed with comparable intensities in both genotypes, and the two groups recovered similarly at day 14 (CFA; Fig. 4a) and week 10 (SNL; Fig. 4b), suggesting that chronic pain-induced hyperalgesia did not differ between genotypes. By contrast, the amplitude and duration of mechanical allodynia were both strongly increased in mutants, and the enhanced mechanical sensitivity of mutant mice was observed in response to both CFA and SNL (Fig. 4c,d). There was otherwise no change in pain sensitivity at contralateral paws or in sham control mice in any chronic pain model (Supplementary Figs. 5 and 6). Together, these results demonstrate that the NR2A-H128S mutation specifically increases mechanical allodynia under conditions of persistent pain. Binding of endogenous Zn^{2+} to the NR2A subunit, therefore, reduces mechanical sensitivity as chronic pain develops.

Why Zn^{2+}-NR2A binding contributes to reduce chronic pain mainly in the mechanical modality remains open. A large body of evidence indicates that NMDARs are overstimulated under conditions of chronic pain[15,16], a phenomenon that influences several signaling pathways[29]. Future studies will determine the main downstream effectors in the pain-reducing effect of zinc, including the well established neuronal cyclooxygenase-2 pathway[30] that is known to modulate mechanical sensitivity[31].

Analgesic effects of exogenous zinc in NR2A-H128S mice

We investigated the analgesic effects of exogenous zinc in WT and NR2A-H128S knock-in mouse littermates (Fig. 5 and Supplementary Figs. 7 and 8). We used the tail flick test, the inflammatory model and the neuropathic pain model. Low doses of zinc were administered to avoid the toxicity associated with high zinc dosage[32]. WT mice responded strongly to zinc. Indeed, both intrathecal and subcutaneous zinc increased tail withdrawal latency in the tail flick test (Fig. 5a,b), in agreement with a previous report[33]. Moreover, zinc administration almost completely reversed thermal hyperalgesia and mechanical allodynia in both CFA (Fig. 5c,d) and SNL (Fig. 5e,f) models of chronic pain. The effect of zinc was observed at a time point at which inflammatory and neuropathic pain had fully developed.

These results confirm that both local and systemic injections of low-dose zinc produce pronounced analgesia in rodents[33–35] and uncover a remarkably robust effect of zinc under conditions of chronic pain.

In contrast, zinc was totally ineffective in NR2A-H128S knock-in mice. Zinc did not modify tail withdrawal responses to acute heat stimulation (Fig. 5a,b). Furthermore, neither thermal nor mechanical responses were altered by zinc administration in both inflammatory (Fig. 5c,d) and neuropathic (Fig. 5e,f) pain models. Overall, the NR2A-H128S mutation abolished all the pain-reducing effects of zinc that were tested. The lack of zinc effects in mutant mice unequivocally demonstrates that binding of high-affinity Zn^{2+} to NR2A subunit is essential for zinc-induced analgesia. These results provide a molecular mechanism for the pain-relieving properties of dietary zinc and strengthen the notion that zinc therapy may successfully treat intractable pain, such as fibromyalgia[36], peripheral neuropathy[37] or other pain abnormalities[38]. The zinc phenotype of mutant mice also reveals a largely unanticipated key role of NR2A-containing receptors in pain processing. The involvement of diheteromeric NR1–NR2A receptors containing two copies of the zinc-sensitive NR2A subunit is most probable. In addition, triheteromeric receptors that incorporate both NR2A and non-NR2A subunits and represent a substantial fraction of NMDARs[39,40] could also contribute, although their zinc sensitivity is lower[41]. There is evidence for the therapeutic utility of NR2B-selective antagonists as analgesics that limit the severe consequences of general NMDAR blockade[14,42]. Our finding calls for new strategies that selectively target zinc-sensitive NR2A-containing receptors for controlling persistent pain states.

DISCUSSION

The striking pain phenotype observed in knock-in NR2A-H128S mice shows that high-affinity Zn^{2+} binding to the NR2A subunit is sufficient to dampen NMDAR function in pain pathways. As the NR2A-H128S mutation eliminates sensitivity of NMDARs to nanomolar,

but not micromolar, zinc concentrations[18–20], our data strongly suggest that extracellular zinc levels that fine-tune NMDAR activity *in vivo* are in the submicromolar range. Endogenous zinc, therefore, regulates NMDAR function at concentrations far lower than previous estimations[2,3]. The origin of zinc diffusing in the vicinity of NMDARs is yet to be determined. Zn^{2+} ions that are stored with glutamate in synaptic vesicles and released during neuronal activity are obvious candidates[23]. Inhibitory GABAergic neurons, which in the spinal cord form a major contingent of zinc-containing terminals[43], may provide additional sources of zinc. Finally, NMDA-dependent spinal long-term potentiation is well recognized as a cellular substrate for hyperalgesia[44] and is blocked by exogenous zinc[4]. Future experiments using NR2A-H128S mutant mice will determine the role of endogenous zinc acting at NR2A subunits in spinal plasticity. Altogether, our data show that high-affinity Zn^{2+} binding to the NR2A subunit is a fundamental molecular event in principal aspects of pain transmission, chronic pain development and zinc-induced analgesia. This discovery has important implications for pain physiopathology and its management in the clinic.

METHODS

Methods and any associated references are available in the online version of the paper at http://www.nature.com/natureneuroscience/.

ONLINE METHODS

Animal procedures

All experiments were performed in accordance with the European Communities Council Directive of 24 November 1986. Mice were housed in a temperature- and humidity-controlled animal colony on a 12 h dark–light cycle with food and water *ad libitum.* For behavioral studies, mice were around 12 weeks old. Researchers were blind to genotype and treatment during behavioral experiment. All data are presented as means ± s.e.m.

Generation of NR2A-H128S knock-in mice

We generated mice carrying the H128S mutation in the NR2A subunit (Fig. 1a). An 11-kb genomic clone containing exon 1 of the *NR2A* gene (Mouse Genome Database NM008170) was isolated from C57Bl/6 mouse genomic DNA and cloned into pUC18. This clone was engineered to introduce the histidine-to-serine mutation (CAT to TCC) at position 128, a floxed *neo* cassette at the 3′ side and a thymidine kinase plus diphtheria toxin A (DTA)-encoding cassette at 5′ side. The targeting vector was linearized and electroporated into 129/SV-derived embryonic stem cells followed by neomycin selection. Selected colonies were screened for homologous recombination by Southern blotting with either Bsu361 or BamHI digests, using 5′ and 3′ external probes or *neo* probe (Fig. 1a,b). *neo* cassette insertion was screened by long-range PCR. A positive clone was transfected with a Cre recombinase-expressing plasmid to remove the floxed *neo* cassette; removal was verified by PCR. Embryonic stem cells with the correct genotype were injected into C57BL/6 blastocysts, and resulting chimeric males were bred with C57BL/6 females for germline transmission. Heterozygous $NR2A^{H128S/+}$ mice were crossed to generate the homozygous $NR2A^{H128S/H128S}$ mouse line, referred as to NR2A-H128S throughout the study. To confirm

the NR2A-H128S mutation, genomic DNA from mutated mice was PCR-amplified and confirmed by DNA sequencing (Fig. 1c). Genotyping of NR2A-H128S mutant mice was performed as for embryonic stem cell screening. The 35-bp difference between knock-in and WT alleles resulted from the remaining *loxP* site in the knock-in allele. Forward primers that were used were 5′-TCATCCCCATCTTGGGCATTCAT-3′ for WT DNA and 5′-TCATCCCCATCTTGGGCATTTCC-3′ for knock-in DNA, and the reverse primer was 5′-AGCATCTGAGTACCCCATCTTCAAA-3′ (Fig. 1d). All experimental mice (WT and knock-in) were on a 50% C57BL/6J, 50% 129/SV genetic background and were littermates obtained by crossing heterozygous *NR2A*$^{H128S/+}$ breeders.

Chmicals and drugs

2,3-Dihydroxy-6-nitro-7-sulfamoyl-benzo[f]quinoxaline-2,3-dione (NBQX), bicuculline methochloride, D-(−)-2-amino-5-phosphonovaleric acid (D-APV), QX-314 and tetrodotoxin were from Ascent Scientific. Mouse TIP39 was from Phoenix Pharmaceuticals. Zinc chloride, 1,2-bis (*o*-aminophenoxy)ethane-*N*,*N*,*N*′,*N*′-tetraacetic acid (BAPTA), diethylene-triaminepentaacetic acid (DTPA) and all other compounds were from Sigma. Ifenprodil and Ro 25-6981 were generous gifts from Sanofi-Synthélabo and Hoffmann-La Roche, respectively.

Transplantation of mouse brain membranes into *Xenopus laevis* oocytes and measurements of NMDA currents

Forebrain membranes were prepared and injected into *Xenopus laevis* oocytes following the protocol adapted from ref. 45. To summarize: using a Teflon glass homogenizer, ~0.5 g of forebrain from 5-week-old mice was homogenized in 4 ml glycine buffer A (200 mM glycine, 150 mM NaCl, 50 mM EGTA, 50 mM EDTA and 300 mM sucrose, pH 9.0 with NaOH) plus protease inhibitors (1:1,000 (vol/vol) pepstatin 10 mg ml^{-1}, 1:1,000 (vol/vol) leupeptin 10 mg ml^{-1} and three additions of 20 μl phenylmethanesulfonylfluoride 150 mM). The homogenate was centrifuged at 9,500*g* for 10 min at ~20 °C. The supernatant was centrifuged for 2 h at 130,000*g* (4 °C). The pellet was washed with 4 ml glycine buffer B (5 mM glycine and 1 mM EDTA, pH 7.5 with NaOH), resuspended in 200 μl glycine buffer B, and divided into 10-μl aliquots that were quickly frozen on dry ice and kept at −80 °C. Immediately before use, membrane samples were thawed and directly injected into defolliculated oocytes (~50 nl per oocyte, ~10 mg protein per ml). NMDA currents were recorded (−60 mV) 1 or 2 d after injection, by applying saturating concentrations of NMDA (300 μM) and glycine (100 μM) to the extracellular perfusion solution. Strychnine (10 μM) was also added to avoid inhibitory glycine receptor activation. Oocyte preparation, injection, voltage-clamping and superfusion methods are the same as previously described[18,19]. In zinc sensitivity experiments, tricine (*N*-tris (hydroxymethyl)methylglycine, 10 mM) was used to buffer zinc[17], following the relationship[17,19] $[Zn]_{free} = [Zn]_{added}/200$. In ifenprodil sensitivity experiments, DTPA (10 μM) was added to chelate trace amounts of heavy metals[17]. Recordings were performed at ~20 °C.

Patch-clamp recordings of synaptic NMDA currents

Hippocampal slice preparation—Acute horizontal hippocampal slices were prepared from 3- to 4-week-old mice. Mice were anesthetized with sodium pentobarbital (30 mg kg^{-1}) and decapitated, and brains were placed in ice-cold artificial cerebrospinal fluid (ACSF) containing 125 mM NaCl, 26 mM $NaHCO_3$, 2.5 mM KCl, 1.25 mM NaH_2PO_4, 2 mM $CaCl_2$, 1 mM $MgCl_2$ and 20 mM glucose bubbled with 95% O_2 and 5% CO_2. Slices (320 μm thick) were cut in ice-cold ACSF supplemented with 50 μM D-APV.

Spinal cord slice preparation—Under sodium pentobarbital anesthesia, 3-week-old mice were decapitated and the spinal cords were removed by hydraulic extrusion. Transverse slices (290 μm thick) were cut mainly from the lumbar segment in ice-cold solution (130 mM potassium gluconate, 15 mM KCl, 0.2 mM EGTA, 20 mM HEPES and 25 mM glucose, pH 7.4 with NaOH) supplemented with 50 μM D-APV, 0.5 μM tetrodotoxin and 50 nM minocycline.

Recording conditions, data acquisition and analysis—Slices were transferred to a recording chamber perfused with bubbled ACSF and visualized in the transmitted deep red light (~750 nm) using a CoolSnap CCD camera (Photometrics).

Patch pipettes were filled with intracellular solution containing 125 mM cesium gluconate, 20 mM BAPTA, 5 mM QX-314, 5 mM tetraethylammonium chloride, 10 mM HEPES, 4 mM Mg-ATP and 0.2 mM Na-GTP, pH 7.3 with CsOH. Pipette resistance was between 4 and 8 MΩ.

For hippocampal recordings, whole-cell voltage-clamp recordings of excitatory postsynaptic NMDA receptor–mediated currents (NMDA EPSCs) were obtained from CA1 pyramidal cells by stimulating the Schaeffer collateral input in the presence of tricine (10 mM), 2,3-dihydroxy-6-nitro-7-sulfamoylbenzo[f]quinoxaline-2,3-dione (NBQX; 10 μM) and bicuculline (10 μM). To avoid antidromic CA3 stimulation, we cut between the CA3 and CA1 regions. For spinal cord recordings, NMDA EPSCs were obtained from dorsal horn lamina II cells by focal stimulation of the tissue in a perimeter 50–100 μm around the patched cell. Lamina II cells were recorded in presence of tricine (10 mM), NBQX (10 μM), bicuculline (10 μM), strychnine (1 μM) and RO-256981 (1 μM) to minimize the contribution of putative presynaptic NR2B-containing NMDA receptors[46,47]. Cells were held at +40 m V. Stimulation pipettes were filled with HEPES-buffered solution and stimulation pulses provided at 0.1 Hz. Intensities of stimuli ranged from 0.4 to 8 mA, and durations of stimuli were 0.1 ms and 0.3 ms for hippocampal and dorsal horn recordings, respectively. Zinc was buffered using 10 mM tricine (see above).

Recordings were performed at 35 °C (hippocampal slices) or 26 °C (spinal cord slices) using an EPC 10 amplifier run with Patch Master software (HeKa Elektronic). Data were acquired at 10 or 20 kHz and filtered at 3 kHz. Series resistance was monitored regularly during recording and compensated at 60–70%. Data were analyzed using NeuroMatic (http://www.neuromatic.thinkrandom.com/) in the IGOR-Pro environment (WaveMetrics). Student's *t*-test was used for statistical comparisons.

Western blots—Three-month-old mice were anesthetized with sodium pentobarbital and decapitated. Forebrains were dissected in ice-cold Mg-ACSF (ACSF with $CaCl_2$ and $MgCl_2$ concentrations swapped). Thoracic and lumbar portions of spinal cords were rapidly removed by hydraulic extrusion in Mg-ACSF. Isolated forebrains and spinal cords were homogenized with a Teflon glass homogenizer in 500 µl buffer 1 (320 mM sucrose and 5 mM HEPES pH 7.4, plus a protease inhibitor cocktail tablet (Complete, Mini; Roche)). After 200 µl buffer 1 addition, cells, nuclei and debris were removed by centrifugation twice at 1,000*g* for 10 min, 4 °C. Enriched membrane fractions were collected by supernatant centrifugation at 100,000*g* for 30 min, 4 °C. Pellets were resuspended in 500 µl buffer 2 (5 mM Tris-HCl, pH 8.1, 0.5% Triton X-100 and protease inhibitors). Preparations were used immediately for immunodetection experiments or stored at −80 °C.

Mouse forebrains and spinal cord samples were separated in nonreducing conditions by 4–12% SDS-PAGE, dry-transferred to nitrocellulose membrane and immunoblotted with the following antibodies: anti-NR1 (1:1,000, mouse monoclonal clone 54.1, Millipore), anti-NR2B (1:100, mouse monoclonal clone 13, BD Transduction), anti-NR2A (1:500, rabbit monoclonal clone A12W, Millipore), anti-GluR1 (1:300, rabbit polyclonal, Millipore), anti-ZnT3 (1:100, kindly provided by Victor Faundez), anti-GlyRα1 (1:1,000, monoclonal mouse antibody 4a, Synaptic Systems) and anti-α-tubulin (1:5,000, mouse monoclonal clone DM1A, Millipore) to normalize proteins signals. Proteins bands were visualized using secondary peroxidase-linked goat anti-rabbit or anti-mouse (1:10,000, Jackson ImmunoResearch), with the SuperSignal West Pico Chemiluminescent Substrate (Thermo Scientific).

Western blot quantification was performed using the US National Institutes of Health ImageJ software. For each protein and given WT–knock-in mouse pair, band intensities between WT and knock-in (KI) samples were compared and normalized to the intensity ratio between respective α-tubulin signals: protein ratio KI/WT = $(\text{protein}_{KI}/\text{protein}_{WT}) \times (\text{tubulin}_{WT}/\text{tubulin}_{KI})$. This procedure was repeated several times using different pairs and mean protein ratio (KI/WT) calculated. Statistics were performed using a one-sample Student's *t*-test.

Timm's staining—Mice 3 weeks or 3 months old were anesthetized with 7% chloral hydrate and intracardially perfused with the following successive solutions: 0.9% (wt/vol) NaCl, Timm's solution (24 mM Na_2S and 43 mM NaH_2PO_4) and finally 4% (wt/vol) paraformaldehyde in 0.1 M phosphate buffer (PFA-PB, pH 7.2) at ~4 °C. Brains were dissected and postfixed in PFA-PB overnight at 4 °C and cut in 50-µm coronal slices with a vibratome in cold PBS (Euromedex). Sections were rehydrated, mounted on gelatin-coated slides and developed for 45 min in the dark at ~20°C in a solution comprising 60 ml 50% (wt/vol) gum arabic, 10 ml 2 M citrate buffer, 30 ml 0.5 M hydroquinone and 1 ml 1 M silver nitrate. After rinsing, slides were placed in 30% (wt/vol) sodium thiosulfate solution, rinsed again in bi-distilled water, dehydrated and finally coverslipped.

Neurological examinations—The general health of mice was evaluated by measuring body weight, body temperature and overt behavioral signs (coat appearance, body posture

and secretory signs). Sensory functions were evaluated by scoring 0 for no response and 1 for a response.

Visual ability—Orientation responses to a moving object (a cotton swab) in each peripheral visual field at a distance of 5 cm were assessed.

Audition—Preyer and startle reflexes (pinna flicking backwards and startle) to a 90-dB click noise of 20 kHz frequency and acoustic startle was tested.

Olfaction—Olfactory exploration of an object (a cotton swab) presented in front of the mouse's muzzle was examined.

Tactile perception—Tactile perception was evaluated by the reaction to pinna and corneal touch using a cotton wire.

Motor functions were evaluated as follows:

Rotarod test—Mice were submitted to three Rotarod (Bioseb) test trials separated by 5 to 10 min intervals and during the tests, the speed of rotation was accelerated from 4 to 40 r.p.m. in 5 min. The falling latency was recorded.

String test—The apparatus was a wire stretched horizontally 40 cm above a table. Testing consisted of three consecutive trials separated by 5-min intervals. On each trial the mouse's forepaws were placed on the wire and the falling latency recorded, with a 60-s cut-off.

Grip test—The maximal muscle strength was measured using an isometric dynamometer connected to a grid (Bioseb). Once the mouse had gripped the grid with its forepaws, it was slowly pulled back until released. The maximal strength developed was recorded.

Locomotor activity and rearing—Mice were tested in automated open fields (Panlab). The open fields were placed in a homogeneously illuminated room (150 lux). Each mouse was placed in the periphery of the open field and allowed to explore freely for 30 min. The distance traveled and the rearing number was recorded over the test session.

Locomotor habituation, circadian activity and food consumption—Spontaneous locomotor activity and food consumption were measured with an electronic monitoring system (Imetronic). Each testing box consisted of a detachable cage equipped with a food magazine, drinking bottle and infrared sensors to measure ambulatory locomotor activity and rears. Food consumption was recorded as the number of 20-mg pellets delivered during the testing by an automated pellet feeder. Mice were placed in the boxes at 11:00 for a 32-h period to measure habituation (first 5 testing hours) as well as nocturnal and diurnal activities. The light in the boxes was on from 07:00 to 19:00 and switched off automatically from 19:00 to 07:00, the same light–dark cycle as in the holding room.

Nociceptive thresholds—Experiments were performed between 09:00 and 15:00, and mice were habituated to the testing area for 20 min. For tail immersion, tail flick and tail

pressure tests, each mouse was lightly restrained in a 50-ml cylinder and habituated twice daily for 3 d.

Tail immersion and tail flick tests—Tail immersion tests were conducted by immersing the tail (5 cm from the tip) into a water bath at 46 °C, 48 °C and 50 °C[48]. The tail flick test was conducted by exposing the tail to radiant heat (Bioseb). For both tests, tail withdrawal latencies were determined with a cut-off of 30 s. To examine the dependency on heating rate of hypersensitivity on tail flick test, heat rates of 0.9 °C s^{-1}, 2.2 °C s^{-1} and 4.0 °C s^{-1} were used. To evaluate zinc-induced analgesia, maximum possible effect (%MPE) was calculated by the following equation: $\%MPE = (latency_{zinc} - latency_{baseline})/(30 - latency_{baseline})$.

Hargreaves test—The radiant heat source (Bioseb) was focused on the plantar surface of the hindpaw[48]. The paw withdrawal latency was measured automatically with a cut-off of 30 s.

Hot plate test—Latency for hindpaw discomfort (jumping, licking and shaking) after putting mice on a 52 °C hot plate (Bioseb) was measured. A cut-off of 120 s was used[48].

Tail pressure test—A gradually increasing pressure was applied to tail using the pressure stimulation unit with a conic tip (Bioseb)[48]. The pressure threshold of tail withdrawal was determined, with a 500 g cut-off value.

Von Frey test—A series of eight von Frey filaments (with bending force of 0.008–2 g) was applied to the hindpaw according to the up-and-down method[48]. The response threshold was calculated by the Excel program generously provided by A. Basbaum (University of California, San Francisco).

Inflammatory pain—Inflammatory pain was induced by intraplantar injection of CFA to the left hindpaw[48]. Response to heat (days 1–14) and mechanical (day 1–24) stimuli was assessed after injection of 4 μl CFA (Fig. 4). For zinc analgesia, pain measurement was performed 2 or 3 d after injection of 8 μl CFA for both heat and mechanical responses (Fig. 5). Pain sensitivity was evaluated using the raw values or percentage pain values, calculated as percentage pain = $(value_{contralateral} - value_{ipsilateral})/value_{contralateral}$.

Neuropathic pain—Neuropathic pain model mice were produced by ligating the left sciatic nerve according to the method previously described[48]. Sham-operated mice were produced by the same surgery without nerve ligation. Response to heat (weeks 1–10) and mechanical (weeks 1–12) stimuli was assessed after the surgery (Fig. 4). For zinc analgesia, pain measurement was performed in weeks 2, 3 for both heat and mechanical responses (Fig. 5). Pain sensitivity was evaluated using the raw or percentage pain values, as described above.

Chemical pain—Intraplantar injection of molecules that preferentially stimulate C fibers[49] (capsaicin) or Aδ fibers[28] (TIP39) was used to assess chemical pain. Mice were habituated in a Plexiglas cage for 30 min before testing. Capsaicin (1.6 μg per 10 μl) or TIP39 (100

pmol per 10 μl) was injected into the plantar surface of the right hind paw. The duration of nociceptive responses (licking, biting and shaking) was recorded for 10 min.

Zinc administration—Zinc chloride was dissolved in 0.9% saline and injected intrathecally or subcutaneously. To examine the zinc antinociception, zinc solution was injected 30 min before the first measurement and the effect was measured each 30 min until 240 min after injection. To examine zinc antihyperalgesia and antiallodynia, zinc solution was injected 90 min before the testing.

Statistical analysis for behavioral measurements

Neurological assessment—Data were analyzed using Student's *t*-test (except Rotarod and string tests) or the non-parametric Mann-Whitney *U*-test.

Locomotor habituation and circadian activity—Two-way ANOVA with genotype as the independent factor and time as the repeated measure was used. Student's *t*-test was used for individual group comparisons of total activity.

Pain—The comparison between genotypes for acute nociception, inflammatory and neuropathic pain was analyzed using repeated measures ANOVA, followed by Student's *t*-test for individual time points when appropriate. The analysis of zinc pharmacology was performed using two-way ANOVA for zinc effect and genotype followed by the Bonferroni-Dunn test.

Supplementary Material

Refer to Web version on PubMed Central for supplementary material.

Acknowledgments

We thank B. Puvion, A. Matifas and R. Weibel for technical assistance and E. Krejci for help with the targeting vector. We thank B. Barbour, J. Becker and E. Schwartz for comments on the manuscript. We also thank Victor Faundez (Emory University) for the gift of the ZnT3 antibody. This research was supported by the Centre National de la Recherche Scientifique (CNRS), Institut National de la Santé et de la Recherche Médicale (INSERM), the Université de Strasbourg, the Agence Nationale de la Recherche (France) grant SynapticZinc (P.P. and B.K.), the US National Institutes of Health, National Institue on Drug Abuse grant DA05010 (B.K.) and an Equipe Fondation pour la Recherche Médicale (FRM) grant (P.P.). C.N. was supported by the FRM and A.M.V. by the Région Ile-de-France.

References

1. Hambidge KM, Krebs NF. Zinc deficiency: a special challenge. J Nutr. 2007; 137:1101–1105. [PubMed: 17374687]
2. Frederickson CJ, Suh SW, Silva D, Thompson RB. Importance of zinc in the central nervous system: the zinc-containing neuron. J Nutr. 2000; 130:1471S–1483S. [PubMed: 10801962]
3. Vogt K, Mellor J, Tong G, Nicoll R. The actions of synaptically released zinc at hippocampal mossy fiber synapses. Neuron. 2000; 26:187–196. [PubMed: 10798403]
4. Ma JY, Zhao ZQ. The effects of Zn^{2+} on long-term potentiation of C fiber-evoked potentials in the rat spinal dorsal horn. Brain Res Bull. 2001; 56:575–579. [PubMed: 11786244]
5. Ueno S, et al. Mossy fiber Zn^{2+} spillover modulates heterosynaptic N-methyl-D-aspartate receptor activity in hippocampal CA3 circuits. J Cell Biol. 2002; 158:215–220. [PubMed: 12119362]

6. Kodirov SA, et al. Synaptically released zinc gates long-term potentiation in fear conditioning pathways. Proc Natl Acad Sci USA. 2006; 103:15218–15223. [PubMed: 17005717]
7. Hirzel K, et al. Hyperekplexia phenotype of glycine receptor alpha1 subunit mutant mice identifies $Zn(^{2+})$ as an essential endogenous modulator of glycinergic neurotransmission. Neuron. 2006; 52:679–690. [PubMed: 17114051]
8. Sensi SL, Paoletti P, Bush AI, Sekler I. Zinc in the physiology and pathology of the CNS. Nat Rev Neurosci. 2009; 10:780–791. [PubMed: 19826435]
9. Velázquez RA, Cai Y, Shi Q, Larson AA. The distribution of zinc selenite and expression of metallothionein-III mRNA in the spinal cord and dorsal root ganglia of the rat suggest a role for zinc in sensory transmission. J Neurosci. 1999; 19:2288–2300. [PubMed: 10066279]
10. Jo SM, Danscher G, Schroder HD, Suh SW. Depletion of vesicular zinc in dorsal horn of spinal cord causes increased neuropathic pain in mice. Biometals. 2008; 21:151–158. [PubMed: 17570038]
11. Smart TG, Hosie AM, Miller PS. Zn2+ ions: modulators of excitatory and inhibitory synaptic activity. Neuroscientist. 2004; 10:432–442. [PubMed: 15359010]
12. Frederickson CJ, Koh JY, Bush AI. The neurobiology of zinc in health and disease. Nat Rev Neurosci. 2005; 6:449–462. [PubMed: 15891778]
13. Paoletti P, Vergnano AM, Barbour B, Casado M. Zinc at glutamatergic synapses. Neuroscience. 2009; 158:126–136. [PubMed: 18353558]
14. Traynelis SF, et al. Glutamate receptor ion channels: structure, regulation, and function. Pharmacol Rev. 2010; 62:405–496. [PubMed: 20716669]
15. Woolf CJ, Salter MW. Neuronal plasticity: increasing the gain in pain. Science. 2000; 288:1765–1769. [PubMed: 10846153]
16. Latremoliere A, Woolf CJ. Central sensitization: a generator of pain hypersensitivity by central neural plasticity. J Pain. 2009; 10:895–926. [PubMed: 19712899]
17. Paoletti P, Ascher P, Neyton J. High-affinity zinc inhibition of NMDA NR1–NR2A receptors. J Neurosci. 1997; 17:5711–5725. [PubMed: 9221770]
18. Paoletti P, et al. Molecular organization of a zinc binding n-terminal modulatory domain in a NMDA receptor subunit. Neuron. 2000; 28:911–925. [PubMed: 11163276]
19. Fayyazuddin A, Villarroel A, Le Goff A, Lerma J, Neyton J. Four residues of the extracellular N-terminal domain of the NR2A subunit control high-affinity Zn^{2+} binding to NMDA receptors. Neuron. 2000; 25:683–694. [PubMed: 10774735]
20. Low CM, Zheng F, Lyuboslavsky P, Traynelis SF. Molecular determinants of coordinated proton and zinc inhibition of N-methyl-D-aspartate NR1/NR2A receptors. Proc Natl Acad Sci USA. 2000; 97:11062–11067. [PubMed: 10984504]
21. Gielen M, Siegler Retchless B, Mony L, Johnson JW, Paoletti P. Mechanism of differential control of NMDA receptor activity by NR2 subunits. Nature. 2009; 459:703–707. [PubMed: 19404260]
22. Scherrer G, et al. Knockin mice expressing fluorescent delta-opioid receptors uncover G protein-coupled receptor dynamics in vivo. Proc Natl Acad Sci USA. 2006; 103:9691–9696. [PubMed: 16766653]
23. Cole TB, Wenzel HJ, Kafer KE, Schwartzkroin PA, Palmiter RD. Elimination of zinc from synaptic vesicles in the intact mouse brain by disruption of the ZnT3 gene. Proc Natl Acad Sci USA. 1999; 96:1716–1721. [PubMed: 9990090]
24. Basbaum AI, Bautista DM, Scherrer G, Julius D. Cellular and molecular mechanisms of pain. Cell. 2009; 139:267–284. [PubMed: 19837031]
25. Yeomans DC, Pirec V, Proudfit HK. Nociceptive responses to high and low rates of noxious cutaneous heating are mediated by different nociceptors in the rat: behavioral evidence. Pain. 1996; 68:133–140. [PubMed: 9252008]
26. Le Bars D, Gozariu M, Cadden SW. Animal models of nociception. Pharmacol Rev. 2001; 53:597–652. [PubMed: 11734620]
27. Drdla R, Sandkuhler J. Long-term potentiation at C-fibre synapses by low-level presynaptic activity in vivo. Mol Pain. 2008; 4:18. [PubMed: 18507818]

28. Matsumoto M, Kondo S, Usdin TB, Ueda H. Parathyroid hormone 2 receptor is a functional marker of nociceptive myelinated fibers responsible for neuropathic pain. J Neurochem. 2010; 112:521–530. [PubMed: 19891737]
29. Svensson CI, Hua XY, Protter AA, Powell HC, Yaksh TL. Spinal p38 MAP kinase is necessary for NMDA-induced spinal PGE(2) release and thermal hyperalgesia. Neuroreport. 2003; 14:1153–1157. [PubMed: 12821799]
30. Yaksh TL, Hua XY, Kalcheva I, Nozaki-Taguchi N, Marsala M. The spinal biology in humans and animals of pain states generated by persistent small afferent input. Proc Natl Acad Sci USA. 1999; 96:7680–7686. [PubMed: 10393880]
31. Vardeh D, et al. COX2 in CNS neural cells mediates mechanical inflammatory pain hypersensitivity in mice. J Clin Invest. 2009; 119:287–294. [PubMed: 19127021]
32. Hu H, Bandell M, Petrus MJ, Zhu MX, Patapoutian A. Zinc activates damage-sensing TRPA1 ion channels. Nat Chem Biol. 2009; 5:183–190. [PubMed: 19202543]
33. Larson AA, Kitto KF. Manipulations of zinc in the spinal cord, by intrathecal injection of zinc chloride, disodium-calcium-EDTA, or dipicolinic acid, alter nociceptive activity in mice. J Pharmacol Exp Ther. 1997; 282:1319–1325. [PubMed: 9316841]
34. Safieh-Garabedian B, et al. Zinc reduces the hyperalgesia and upregulation of NGF and IL-1 beta produced by peripheral inflammation in the rat. Neuropharmacology. 1996; 35:599–603. [PubMed: 8887968]
35. Liu T, Walker JS, Tracey DJ. Zinc alleviates thermal hyperalgesia due to partial nerve injury. Neuroreport. 1999; 10:1619–1623. [PubMed: 10380992]
36. Sendur OF, Tastaban E, Turan Y, Ulman C. The relationship between serum trace element levels and clinical parameters in patients with fibromyalgia. Rheumatol Int. 2008; 28:1117–1121. [PubMed: 18496697]
37. Head KA. Peripheral neuropathy: pathogenic mechanisms and alternative therapies. Altern Med Rev. 2006; 11:294–329. [PubMed: 17176168]
38. Yoshida H, Tsuji K, Sakata T, Nakagawa A, Morita S. Clinical study of tongue pain: Serum zinc, vitamin B12, folic acid, and copper concentrations, and systemic disease. Br J Oral Maxillofac Surg. 2010; 48:469–472. [PubMed: 19735964]
39. Al-Hallaq RA, Conrads TP, Veenstra TD, Wenthold RJ. NMDA di-heteromeric receptor populations and associated proteins in rat hippocampus. J Neurosci. 2007; 27:8334–8343. [PubMed: 17670980]
40. Rauner C, Kohr G. Triheteromeric NR1/NR2A/NR2B receptors constitute the major N-methyl-D-aspartate (NMDA) receptor population in adult hippocampal synapses. J Biol Chem. 2010; 286:7558–7566. [PubMed: 21190942]
41. Hatton CJ, Paoletti P. Modulation of triheteromeric NMDA receptors by N-terminal domain ligands. Neuron. 2005; 46:261–274. [PubMed: 15848804]
42. Mony L, Kew JN, Gunthorpe MJ, Paoletti P. Allosteric modulators of NR2B-containing NMDA receptors: molecular mechanisms and therapeutic potential. Br J Pharmacol. 2009; 157:1301–1317. [PubMed: 19594762]
43. Danscher G, et al. Inhibitory zinc-enriched terminals in mouse spinal cord. Neuroscience. 2001; 105:941–947. [PubMed: 11530232]
44. Sandkühler J. Understanding LTP in pain pathways. Mol Pain. 2007; 3:9. [PubMed: 17407590]
45. Miledi R, Eusebi F, Martinez-Torres A, Palma E, Trettel F. Expression of functional neurotransmitter receptors in *Xenopus* oocytes after injection of human brain membranes. Proc Natl Acad Sci USA. 2002; 99:13238–13242. [PubMed: 12237406]
46. Boyce S, et al. Selective NMDA NR2B antagonists induce antinociception without motor dysfunction: correlation with restricted localisation of NR2B subunit in dorsal horn. Neuropharmacology. 1999; 38:611–623. [PubMed: 10340299]
47. Ma QP, Hargreaves RJ. Localization of N-methyl-D-aspartate NR2B subunits on primary sensory neurons that give rise to small-caliber sciatic nerve fibers in rats. Neuroscience. 2000; 101:699–707. [PubMed: 11113318]

48. Gaveriaux-Ruff C, et al. Genetic ablation of delta opioid receptors in nociceptive sensory neurons increases chronic pain and abolishes opioid analgesia. Pain. 2011; 152:1238–1248. [PubMed: 21295407]

49. Sakurada T, Katsumata K, Tan-No K, Sakurada S, Kisara K. The capsaicin test in mice for evaluating tachykinin antagonists in the spinal cord. Neuropharmacology. 1992; 31:1279–1285. [PubMed: 1281912]

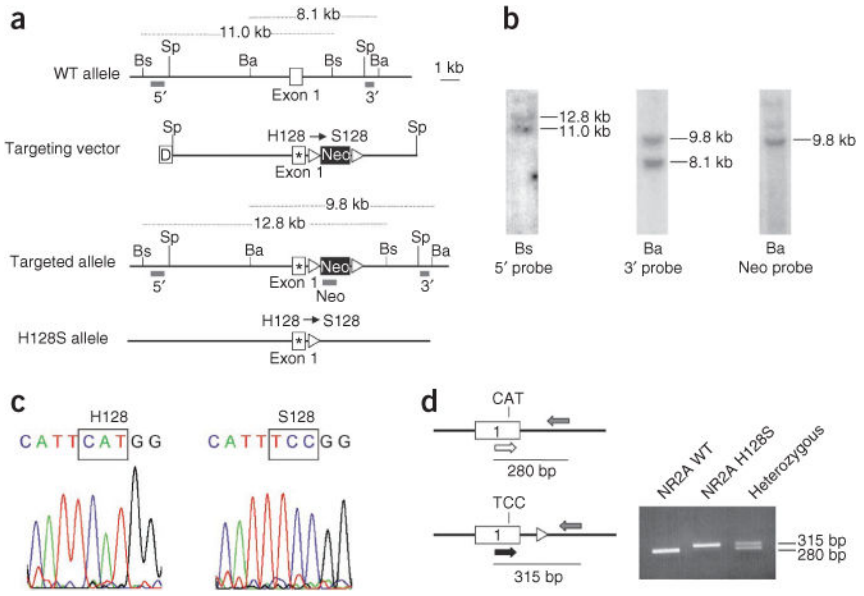

Figure 1.

Targeting the NMDA receptor NR2A subunit gene in mice. (**a**) The NR2A-H128S mutant allele was created by homologous recombination. The scheme shows the WT *NR2A* allele, the targeting vector, the targeted allele and the H128S knock-in allele. The CAT codon encoding histidine 128 (H128) in exon 1 was replaced by the TCC codon encoding serine (S), and a *loxP*-flanked (‘floxed’) *neo* cassette was introduced 3′ from exon 1 to select for embryonic stem cells harboring the knock-in allele. The final mutant allele was obtained after excision of the *neo* cassette by a Cre recombinase treatment of embryonic stem cells. White box, exon 1; star in white box shows the H128S mutation; dark line, intronic sequences; Ba, BamH I; Bs, Bsu361; Sp, SpeI (restriction sites); triangles, *loxP* sites; *neo* box, neomycin-resistance cassette; gray bars, probes for Southern blot analysis; lines above gene indicate expected labeled DNA fragments in Southern blot analysis. (**b**) Southern blot analysis of WT and targeted alleles in the selected embryonic stem cell clone. Genomic DNA was digested with Bsu361 and BamHI, and hybridized with 5′and 3′ external probes, respectively or the *neo* probe. Expected bands at each size as indicated in **a** are obtained. (**c**) Genomic DNA sequence analysis using tail biopsies from WT (left panel) and knock-in homozygous mutant (right panel) mice, showing the replacement of the CAT codon by the mutated TCC codon. (**d**) Genotyping of the NR2A-H128S knock-in line. PCR analysis using mutation-specific primers (strategy on left) reveals WT (280 bp) and mutant (315 bp) alleles (right). White arrow, forward primer for WT DNA, black arrow, forward primer for mutant DNA, gray arrows, reverse primer. Analysis of genomic DNA from WT NR2A, homozygous NR2A-H128S and heterozygous NR2A WT/NR2A-H128S mice is shown. The 35-bp differences between mutant and WT alleles results from the remaining *loxP* site in the mutant allele.

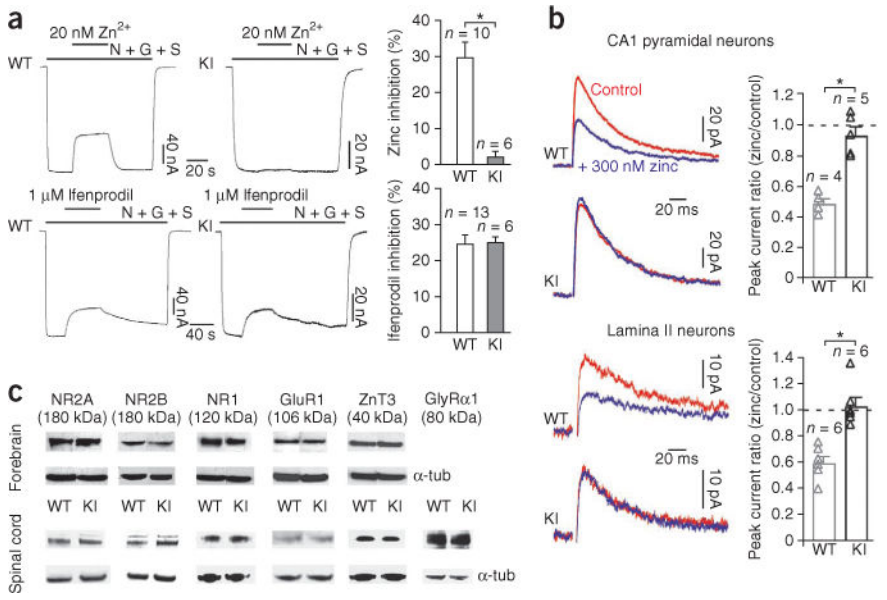

Figure 2.

High-affinity zinc inhibition of NMDA currents is lost in NR2A-H128S mice. (**a**) Sensitivity to subunit-specific modulators of brain NMDARs from WT and knock-in NR2A-H128S (KI) mice transplanted into *Xenopus* oocytes. Inhibition by 20 nM zinc was abolished in KI mice (upper traces; 2.3 ± 1.3%, $n = 6$ versus 30.3 ± 4.2% $n = 10$ for WT; mean ± s.d., $^*P < 0.001$, Student's *t*-test), whereas inhibition by the NR2B-selective antagonist ifenprodil was unchanged (lower traces; 25.2 ± 3.2%, $n = 6$ versus 24.8 ± 2.4% $n = 13$ for WT; $P = 0.7$). NMDA currents were induced by co-application of 300 μM NMDA, 100 μM glycine and 10 μM strychnine (N + G + S). (**b**) Hippocampal Schaeffer collateral to CA1 NMDA EPSCs from KI mice were insensitive to 300 nM zinc, contrasting with the marked inhibition seen in WT mice (peak current ratio: 0.48 ± 0.03 $n = 4$ versus 0.93 ± 0.06 $n = 5$ for KI; $^*P < 0.001$, Student's *t*-test). Same for NMDA EPSCs recorded in the dorsal horn of the spinal cord (0.59 ± 0.05, $n = 6$ for WT versus 1.03 ± 0.07, $n = 6$ for KI; mean ± s.d., $^*P < 0.001$). (**c**) Unaltered protein expression levels in KI mice compared with those of WT mice in forebrain (top) and spinal cord (bottom). Lower band, α-tubulin control (α-tub). Full-length blots are presented in Supplementary Figure 1. For each protein, quantification was performed on two or three different WT-KI couples; no significant changes in expression was detected ($P > 0.05$, one-sample Student's *t*-test; see Supplementary Fig. 2).

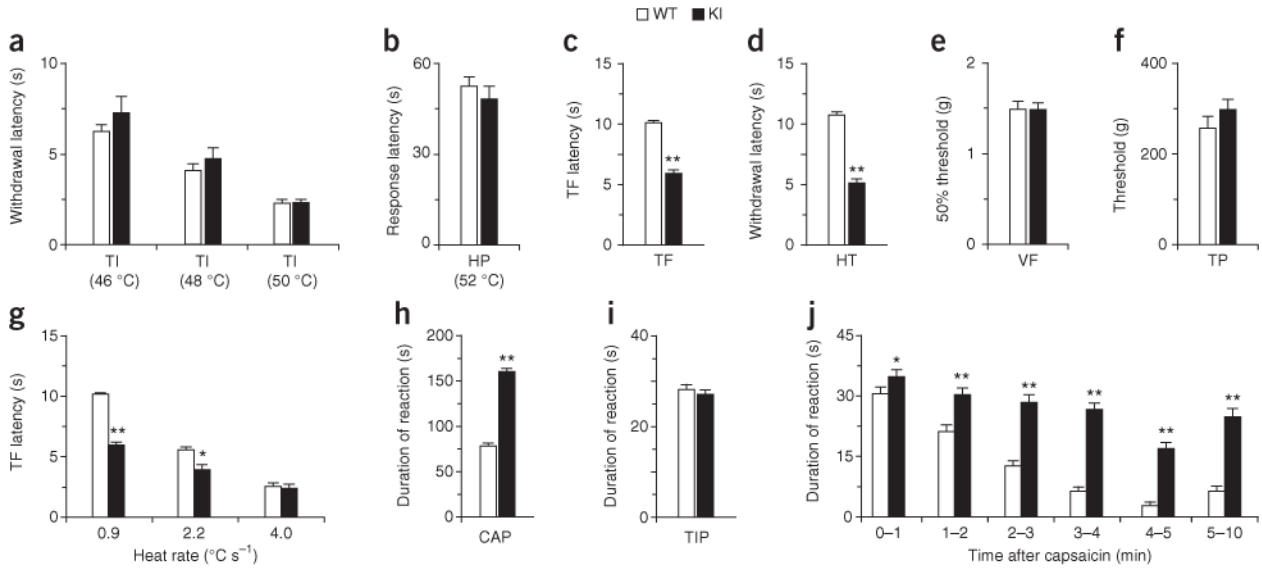

Figure 3.

NR2A-H128S mice show enhanced basal pain sensitivity in response to radiant heat and capsaicin. (**a–j**) Tail immersion (TI), hot plate (HP), tail flick (TF), Hargreaves (HT), von Frey filaments (VF), tail pressure (TP) and chemical tests with capsaicin (CAP) and TIP39 (TIP) were used to evaluate basal pain sensitivity in response to thermal (**a–d**, **g**), mechanical (**e,f**) and chemical (**h–j**) noxious stimuli (see Online Methods). No genotype effect was observed in TI withdrawal at three temperatures (**a**), in the HP response (**b**), in the mechanical responses (**e,f**) or in the TIP response (**i**). By contrast, significant hypersensitivity of NR2A-H128 mice was detected in responses to radiant heat stimuli (**c,d**) and capsaicin (**h,j**). Furthermore, TF test with three different heat rates showed thermal hypersensitivity at 0.9 and 2.2 °C s^{-1} (**g**). Data are expressed as means ± s.e.m. of eight mice per group. **P* < 0.05 and ***P* < 0.001, NR2A-H128S mutants versus controls, Student's *t*-test.

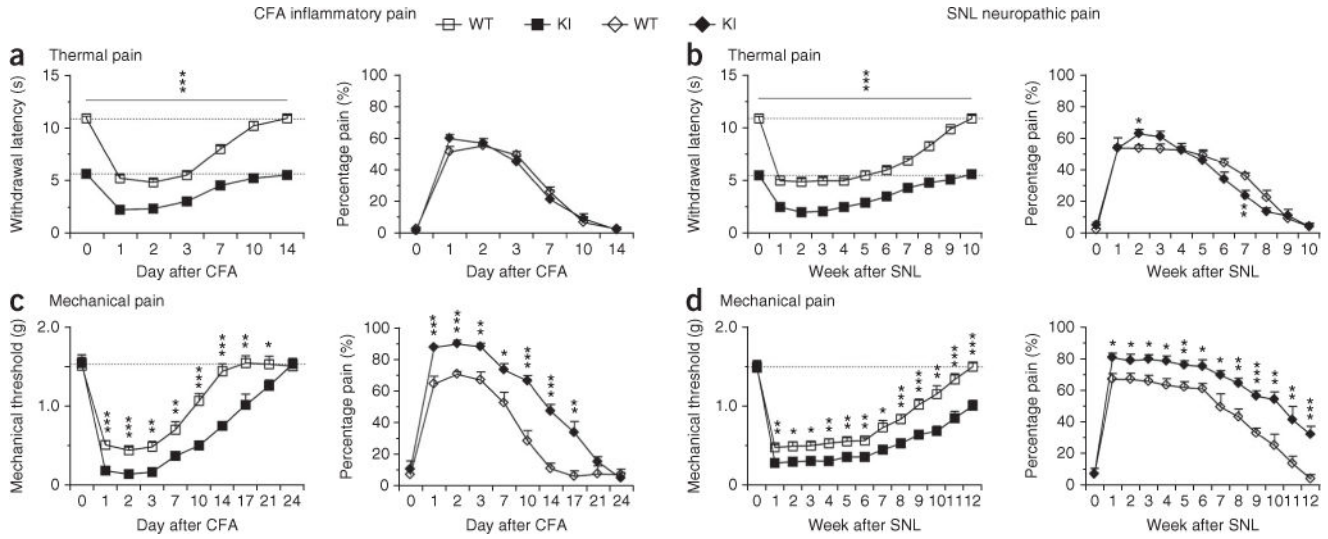

Figure 4.

NR2A-H128S mice show increased mechanical allodynia under chronic pain. Thermal and mechanical sensitivity of mutant knock-in (KI) mice and their WT controls was examined under CFA inflammatory or SNL neuropathic pain. Raw values (left) and percentage pain (right: $(value_{contralateral} - value_{ipsilateral})/value_{contralateral}$) are shown. Dotted line, baseline value. (**a,b**) Thermal sensitivity (Hargreaves test). Areas under the curve (AUC) of percentage pain showed no genotype difference in intensity and duration of thermal hyperalgesia under either CFA (**a**) or SNL (**b**) conditions. (**c,d**) Mechanical sensitivity (von Frey test). Upon CFA injection (**c**), as well as after partial sciatic nerve ligation (**d**), mechanical allodynia developed with higher intensity and duration in mutant mice (AUC of percentage pain: CFA, 316 ± 15 for WT mice versus 510 ± 7.3 for KI mice; SNL, 565 ± 12 for WT mice versus 778 ± 14 for KI mice). Data are expressed as means ± s.e.m. of eight mice per group. *$P < 0.05$, **$P < 0.01$ and ***$P < 0.001$, NR2A-H128S mutants versus controls for individual time points, Student's *t*-test.

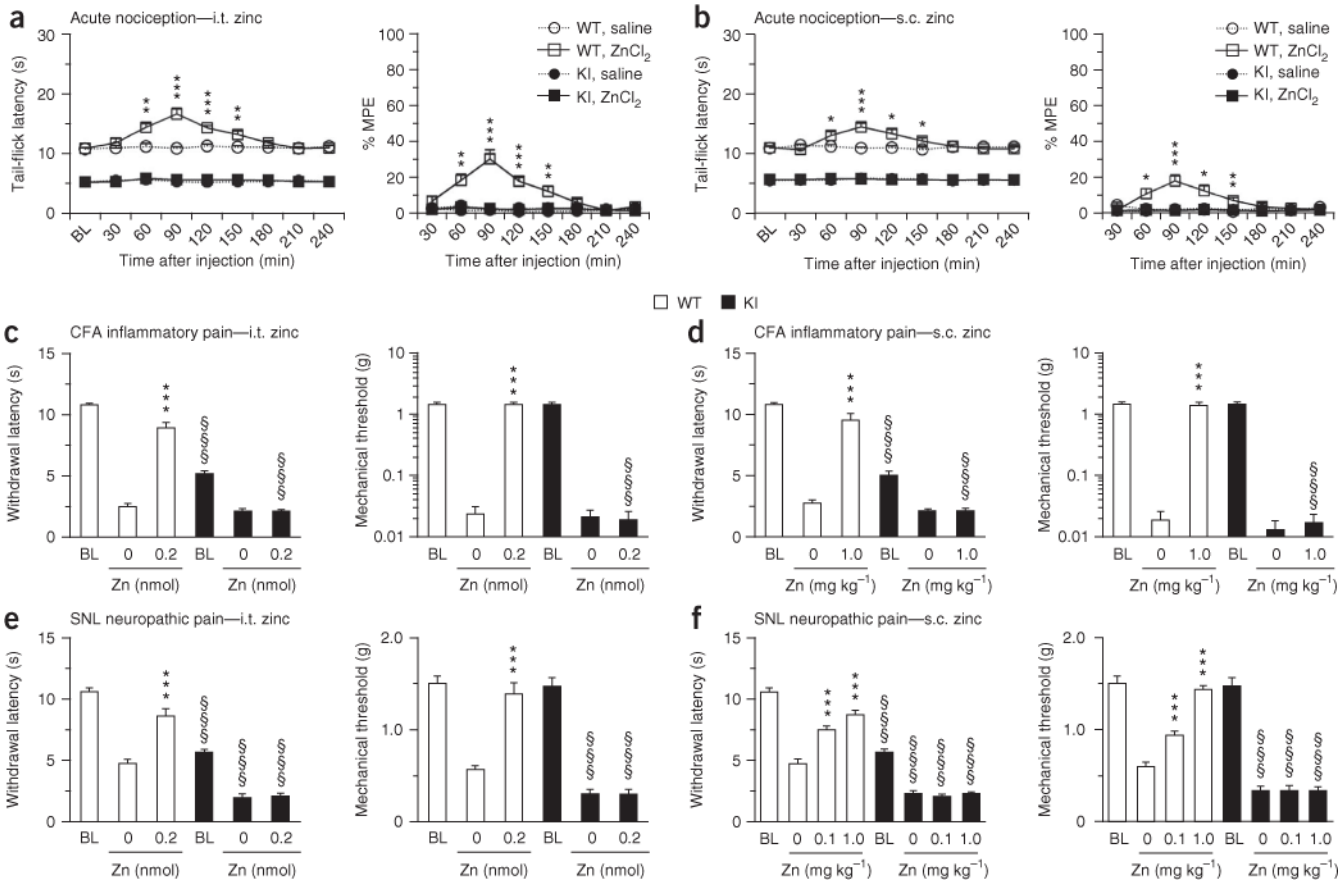

Figure 5.

Zinc analgesia is abolished in NR2A-H128S mice. Zinc analgesia was examined in mutant knock-in (KI) mice and control WT mice after intrathecal (i.t.; 0.2 nM, left panels) or subcutaneous (s.c.; 0.1–1 mg per kilogram body weight, right panels) $ZnCl_2$ administration. Baseline thresholds (BL) were measured in naive mice before the drug injection or induction of chronic pain. (**a,b**) Acute thermal pain (TF; raw values (left panels) and percentage of maximum possible effect (%MPE, right panels; see Online Methods)) shows zinc analgesia in WT but not KI mice. Data are expressed as means ± s.e.m. of eight mice per group. $*P < 0.05$, $**P < 0.01$ and $***P < 0.001$, zinc-treated group versus saline-treated group for individual time points, Student's *t*-test. (c,d) CFA inflammatory pain. Both i.t. or s.c. zinc administrations inhibited CFA-induced thermal hyperalgesia (HT, left panels) and mechanical allodynia (VF, right panels). These antihyperalgesic and antiallodynic effects were absent in mutant mice. (e,f) SNL neuropathic pain. As for inflammatory pain, both i.t. or s.c. zinc inhibited thermal hyperalgesia (HT, left panels) and mechanical allodynia (VF, right panels) induced by sciatic nerve ligation. These antihyperalgesic and antiallodynic effects were absent in KI mice. For both CFA and SNL experimental series, data are expressed as means ± s.e.m. of eight mice per group. $***P < 0.001$ for zinc-treated versus saline-treated groups, $^{§§§}P < 0.001$ for mutants versus controls, two-way repeated measures analysis of variance (ANOVA) followed by Bonferroni–Dunn test.